Effect of heat treatment on the microstructure and mechanical properties of an Al-5Mg_2Si-2Mg alloy processed by laser powder bed fusion

Jianying Wang[1], Feipeng Yang[1], Hailin Yang[1]*, Lijun Zhang[1], Yingying Zhang[1], Zhilin Liu[2], Shouxun Ji[3]

1. State Key Laboratory of Powder Metallurgy, Central South University, Changsha 410083, China

2. Light Alloy Research Institute, College of Mechanical and Electrical Engineering, Central South University, Changsha, 410083, P.R. China

3. Brunel Centre for Advanced Solidification Technology (BCAST), Brunel University London, Uxbridge, Middlesex, UB8 3PH, United Kingdom

* Corresponding authors: y-hailin@csu.edu.cn

Abstract: The response of heat-treatment of an Al-5Mg_2Si-2Mg alloy fabricated by laser assisted powder bed fusion (L-PBF) was investigated for microstructural evolution and mechanical properties. The results showed that the as-LPBFed alloy offered the yield strength of 295 MPa, UTS of 453 MPa and elongation of 9.2%. The solution with and without subsequent ageing is not effective for strength improvement. After solution at 490 ºC for 1 h, the alloy exhibited a striking decrease in strength and increase in elongation, at which the yield strength is 167 MPa, the UTS is 292 MPa and the elongation is 17.3%. With subsequent ageing of solutionised alloy at 180 ºC for 6 h, the yield strength is 179 MPa, the UTS is 295 MPa and the elongation is 13.2 %. On the other hand, direct ageing of L-PBFed alloy significantly improved the strength. After ageing at 180 ºC for 3.5 h, the yield strength of 377 MPa, the UTS of 488 MPa and elongation of 9.6% can be achieved in the alloy, showing 28% increase of yield strength in comparison with as-LPBFed alloy, but still with excellent ductility for engineering applications. It is found that the strength enhancement in the directly as-aged alloy is closely linked to the characteristics of microstructure, which included the refined compact Al-cells, the divorced Mg_2Si eutectics and newly formed ultrafine *in-situ* Mg_2Si particles in the matrix during ageing for precipitation strengthening.

Key words: Aluminium alloys; Microstructure; Mechanical properties; Laser powder bed fusion; Heat treatment

1. Introduction

Al-Mg-Si alloys have been widely used for lightweight applications because of the combined merits of low thermal expansion coefficient, low processing cost, improved specific modulus and strength, and excellent castability [1–4]. The majority of commercially available wrought and cast Al-Si-Mg alloys can be scientifically interpreted as Al-Mg_2Si with extra Si, which provides the fundamentals of strengthening capability through solution and ageing. 0.45–0.65 wt.% Mg are usually dissolved into wrought 6xxx series Al-Si-Mg alloys and even higher in cast Al-Si-Mg alloys [5–9]. However, the excessive addition of Mg in these alloys always leads to the significant loss of ductility due to the limited Mg solution in α-Al matrix and the formation of coarse Mg_2Si phase [5,10].

Recently, aluminium alloys processed by laser-assisted powder bed fusion (L-PBF) have been increasingly attractive to acquire superior mechanical performance with minimal post-processing [11–14]. Generally, aluminium alloys are considered as challenging materials for L-PBF processing because of their high laser reflectivity and thermal conductivity, low melting point, and high sensitivity to hot tearing [15]. Until now, most common Al alloys for L-PBF processing are Al–Si based alloys with high Si contents owing to their narrow solidification range and less defects, mainly including AlSi7Mg, AlSi10Mg, AlSi12 (in wt.%) [16–21]. However, the mechanical properties of these alloys are not satisfied for some engineering applications. For instance, the L-PBFed AlSi12 alloy can offer a tensile strength of ~325 MPa and an elongation of 4.4% [17], and the L-PBFed AlSi10Mg alloy have a tensile strength of ~360 MPa and an elongation of 3.9% under as-LPBFed condition [18]. Although Al-Si alloys have good castability, weldability and hardenability, their strength and ductility are generally poor in comparison with wrought products. To enhance the mechanical properties, the investigations have been focused on the heat treatment of L-PBFed Al alloys. Regrettably, several studies showed that the annealing treatments may deteriorate the mechanical properties of AlSi10Mg and AlSi12 alloys [20,22,23]. It has reported that the solution treatment of AlSi12 alloys at 500 ºC for 4 h can cause a decrease in the yield strength from 230 to 110 MPa and a decrease in the UTS from 360 to 190 MPa [20]. However, the AlSi10Mg alloys with T5 treatment can increase the elongation from 7.8% to 18.7%, but decrease the UTS from 263 MPa to 183 MPa [22]. Recently, investigations for the effect of heat treatment have been extended to other L-PBFed Al alloys including Al-Cu, Al-Zn and Al-Mg based alloys. For instance, an Al-Cu-Mg-Si alloy offers the yield strength of 223 MPa and the elongation of 5.3% under as-LPBFed condition, and that of 368 MPa and 6.2%, respectively, under T6 heat treated condition [24]. Similarly, T6 heat treatment of an L-PBFed

Al-Cu-Mg-Ti alloy can increase the UTS from 365 MPa to 432 MPa, but decrease the elongation from 12% to 10% [25]. On the other hand, the studies of a L-PBFed Al-Mg-(Si)-Sc-Zr alloy showed that the direct ageing at a temperature exceeding 300 ºC can improve the yield strength through the formation of Al_3(Sc, Zr) nanoprecipitates [26,27]. Overall, it is clear that a thorough understanding of the effect of heat treatment on the microstructural evolution and mechanical properties is important for L-PBFed Al alloys.

Based on the experience in die cast alloys [4], the Al-5Mg_2Si-2Mg alloy has been recently processed by L-PBF. The results have shown excellent L-PBF processability and superior mechanical properties [28]. The obvious difference from the commercially available Al-Mg_2Si with extra Si alloys, the Al-5Mg_2Si-2Mg alloy is an Al-Mg_2Si alloy with extra Mg. The response of heat treatment of this alloy is yet unclear after L-PBF processing. Therefore, it is important to understand (*a*) whether the refined Al-Mg_2Si eutectic networks remain in the microstructure after direct ageing and/or solution at high temperatures, and (*b*) whether the effects of solution, solution and ageing, and ageing are effective on the improvement in mechanical properties, such as density, strength and ductility. Consequently, the present work aims to reveal the microstructural evolution and mechanical properties of L-PBFed Al-5Mg_2Si-2Mg alloy after heat treatment including direct ageing, solution, and solution with subsequent ageing. The characterization of microstructural evolution and mechanical properties are described under heat treated condition in comparison with that obtained under as-L-PBFed condition. The discussion focuses on the relationship between the microstructures and the mechanical properties in association with the corresponding strengthening mechanisms.

2. Experimental

2.1 Powder and materials fabrication

Pre-alloyed Al-5Mg_2Si-2Mg powders with a particle size distribution of 15～53 μm were made in house. Inductively coupled plasma atomic emission spectrometry (ICAP 7000 Series) was used to analyse the chemical composition of powders in Table 1. The L-PBF process was conducted using a FS271M (Farsoon, Inc, China) machine. The optimized parameters were adopted with the laser beam spot size of 90 μm, the powder layer of 0.05 mm, the hatch spacing of 0.10 mm, the laser power of 270 W, and the scan speed of 1000 mm/s. The laser scanning strategy was set to be 67º rotating scanning layer-by-layer. More details of powder and materials fabrication can refer to our previous study [28]. By considering the features of L-PBFed alloys containing high gas content and the experience in die cast alloys, the solutionisation temperature was set at 490 ºC [29]. To find out the optimised solutionisation,

the time was varied for 0 – 8 h with immediate water quenching. The subsequent artificial ageing was set at 180 ºC for 0 – 15 h with air cooling. The direct ageing treatment was respectively set at 160 ºC, 180 ºC and 200 ºC for 1 – 12 h with subsequent air cooling.

Table. 1. The composition of experimental Al-5Mg_2Si-2Mg alloy powder calibrated by ICP-AES (in wt.%).

Mg	Si	Mn	Fe	Others	Al
5.13	2.05	0.44	0.11	<0.08	Bal.

2.2 Microstructural characterization and mechanical property

Phase constituent of the samples were examined by X-ray diffraction with Cu K*a* radiation (XRD, Rigaku X-2000). The spectra were recorded in the angular range of 30-80º (2θ) with the step of 0.05º. The microstructural evolution was examined using an optical microscope (OM, Leica DM4000 M), a field emission scanning electron microscope (FE-SEM, FEI nano230), an electron backscattered diffraction (EBSD, FIB Helios NanoLab G3 UC), and a transmission electron microscope (TEM, Tecnai G2 F20). SEM was performed at the acceleration voltage of 10 kV and the working distance of 5 mm. The samples were mechanically polished and etched using Keller's solution before SEM examination. EBSD measurements were carried out at the acceleration voltage of 30 kV with the step size of 0.8 μm, and the corresponding grain sizes were analysed by the TSL OIM software. TEM analysis was conducted at the acceleration voltage of 300 kV, and TEM samples were finalised by using a precision ion polishing system (PIPS) at the voltage of 5 kV/2 kV and the incident angle of 3º ~ 8º.

A FA1104J density instrument was used to measure the density of the samples according to Archimedes principle. Dog-bone-shaped samples with the gauge length of 30 mm were used for tensile testing, which was performed at room temperature using a MTS Alliance RT30 system with the engineering strain rate of 1×10^{-3} s^{-1}. Square shaped samples (10 mm × 10 mm × 2 mm) were used for testing the micro-hardness using a Vickers hardness (ASTM E384-08) under a load of 300 g for 10 s. Each reported data is the average value of at least 5 measurements.

3. Results

3.1 Effect of solution and ageing process on mechanical properties and microstructure

The Vickers hardness of L-PBFed Al-5Mg_2Si-2Mg alloy under as-solutionised only and solution + aged conditions are shown in Fig. 1a. After solutionised at 490 ºC for 1 h, the

hardness decreased significantly from 160.5 Hv to 60.2 Hv, and then the hardness maintained at a level of 60 Hv with increasing the solution time. Furthermore, the samples after solution at 490 ºC for 1 h were aged at 180 ºC for different times. It is seen that, in comparison with the as-solutionised samples, the hardness increased slightly to a level of 65 Hv after ageing. However, the subsequent enhancement became insignificant with prolonged ageing times. The hardness was maintained at a level of 65 Hv after ageing 15 h at 180 ºC.

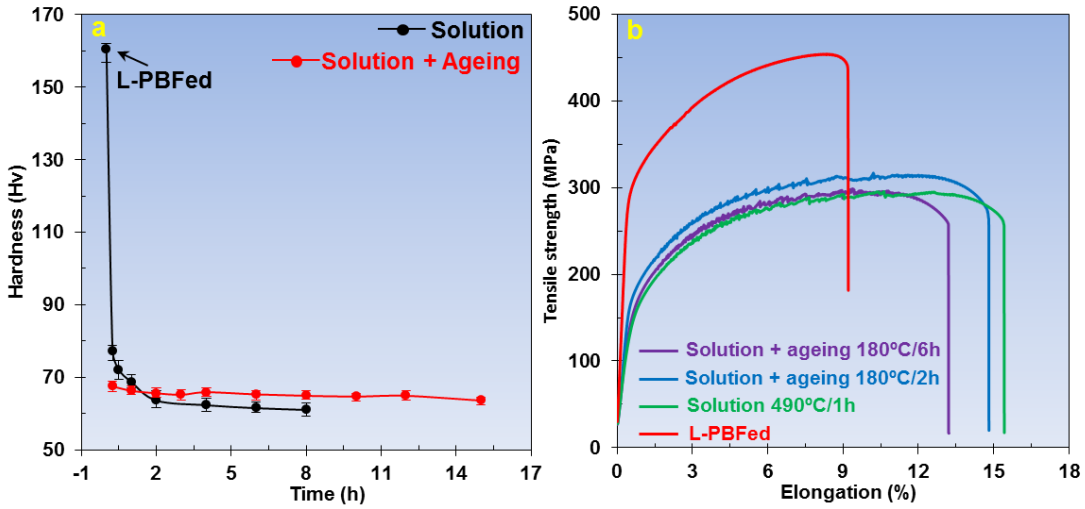

Fig. 1. Effects of solution only and solution plus ageing on (a) the hardness and (b) the tensile strength of Al-5Mg_2Si-2Mg alloy.

The tensile curves of the alloy after solution with and without ageing are shown in Fig. 1b. The as-LPBFed alloy offered the yield strength of 295 MPa, UTS of 453 MPa and elongation of 9.2%. After solution at 490 ºC for 1 h, the alloy exhibited a striking decrease in strength, at which the yield strength was 167 MPa, the UTS was 292 MPa and the elongation was 17.3%. After subsequent ageing at 180 ºC for 2 h for solutionised sample, a slight improvement was achieved, which was 191 MPa of the yield strength, 314 MPa of the UTS and 14.8% of the elongation. Clearly, the yield strength and UTS were basically maintained at the similar levels for all three experimental conditions. Therefore, the heat-treatment process of solution and subsequent ageing cannot remarkably enhance the mechanical properties of the L-PBFed Al-5Mg_2Si-2Mg alloy.

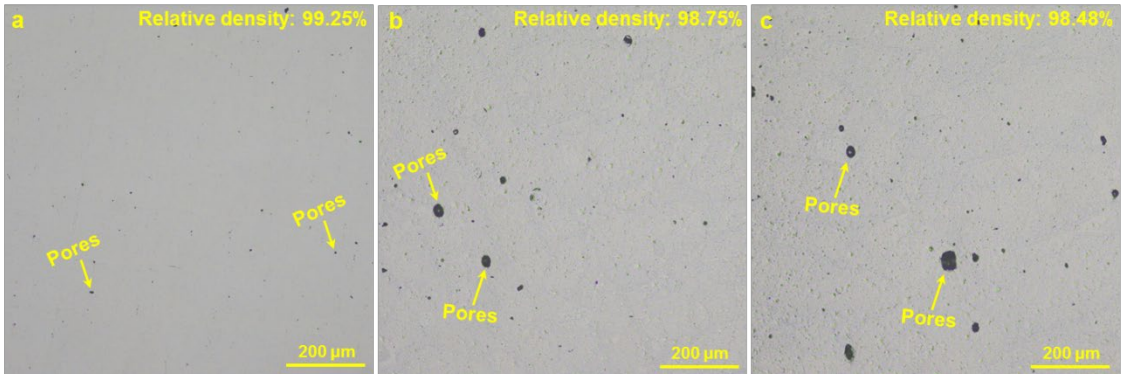

Fig. 2. Optical microscopes (OM) showing the feature of porosity in the cubic sample along the horizontal direction (in cross plane parallel to the base plate) of the Al-5Mg_2Si-2Mg alloy under different conditions ; (a) under as-L-PBFed condition, (b) solutionised at 490 ºC for 1 h, and (c) solutionised and aged at 180 ºC for 2 h.

The optical micrographs of L-PBFed Al-5Mg_2Si-2Mg alloy without and with subsequent solution and ageing are shown in Fig. 2. After solution at 490 ºC/1 h and subsequent ageing, the number density of porosity increased significantly, resulting in the decrement in relative density, as shown in Figs. 2b and 2c. The relative density of the L-PBFed samples was 99.25% under as-LPBFed condition. The mean value of the relative density decreased to 98.75% under as-solutionised condition and 98.48% under as-solutionised + aged condition.

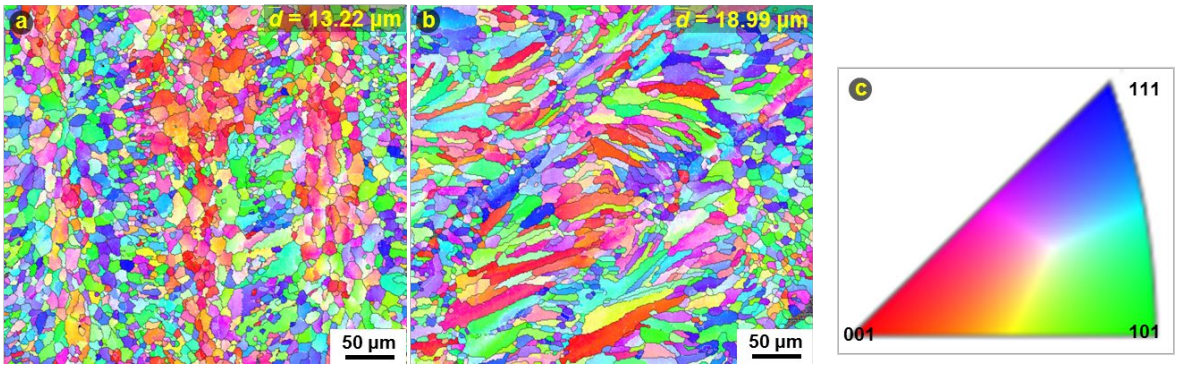

Fig. 3. EBSD images of as-LPBFed Al-5Mg_2Si-2Mg alloy along (a) the horizontal direction (in cross plane parallel to the base plate), (b) the building direction (in cross plane perpendicular to the base plate), and (c) corresponding IPF map.

EBSD images along the horizontal and building directions in the as-LPBFed Al-5Mg_2Si-2Mg alloy are shown in Fig. 3. The microstructure along the horizontal direction was mainly composed of equiaxed grains with numerous fine primary α-Al grains at a level of 1 µm in the local area. Along the building direction, grains were found in columnar morphology and the size ranged from 100 to 200 µm in length and from 1 to 20 µm in width, as shown in Figs. 3a and 3b. Additionally, it is observed that local regions in the conjunction areas of columnar grains contained fine equiaxed α-Al grains. Meanwhile, the average sizes of grains along two

directions were 13.22 μm and 18.99 μm, respectively. Moreover, Fig. 4 shows the detailed characteristics of the Al-5Mg_2Si-2Mg alloy along the horizontal direction (Figs. 4a-c) and the building direction (Figs. 4d-f). It is seen that a melting pool (MP) coarse zone was observed in the L-PBFed alloy along both directions. The microstructure on the cross sections exhibited a bimodal feature for primary α-Al grains, including the coarse equiaxed Al-cells at the melting pool boundaries and the fine equiaxed Al-cells along the thermal gradient towards the top-centre of melting pools. Particularly, a heat affected zone (HAZ) was found between the coarse MP zone and the MP fine zone along the building direction. Two obvious differences were observed in the two directions, including that the equiaxed Al-cells in the horizontal direction (Fig. 4e) were significantly coarser than that in the building direction (Fig. 4b), and that the columnar Al-cells along the building direction exhibited fibre-like morphology (Fig. 4f).

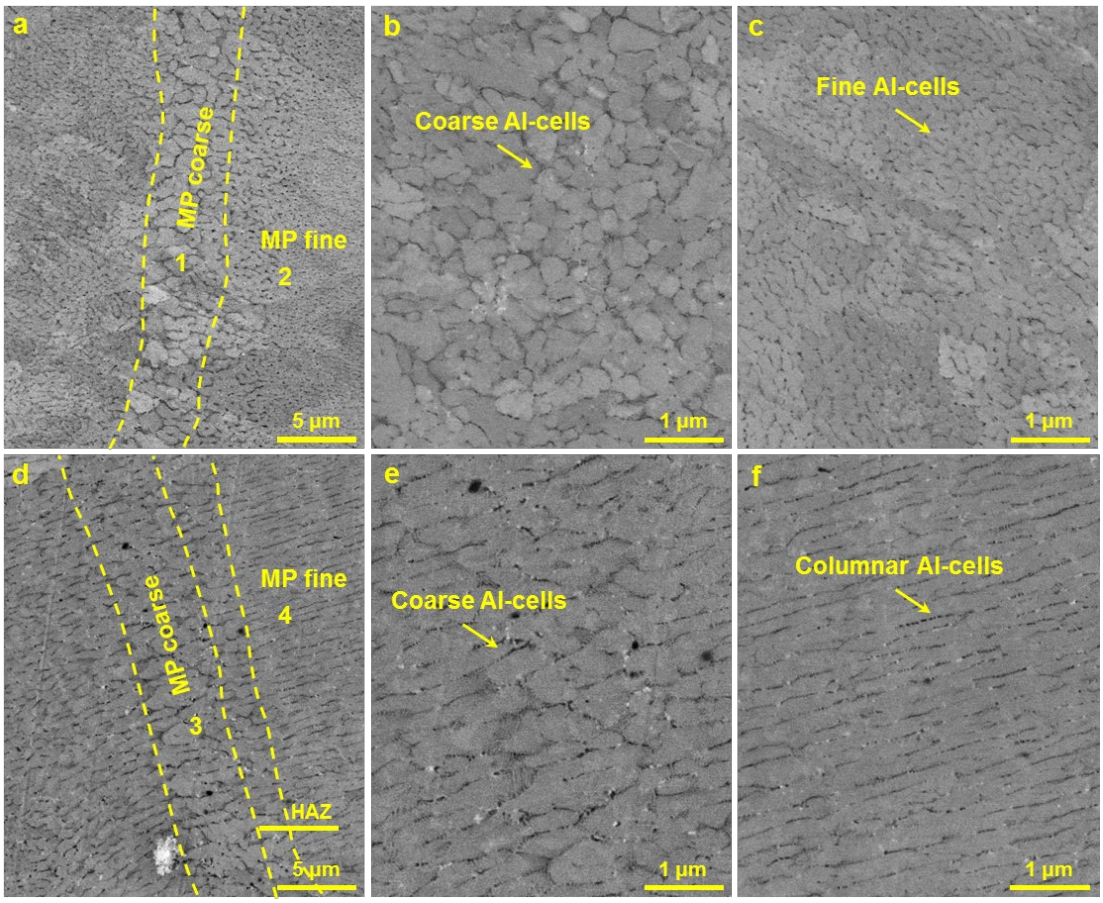

Fig. 4. SEM images of as-LPBFed Al-5Mg_2Si-2Mg alloy showing (a) the overall microstructure, (b) the detailed microstructure in zone 1, and (c) the detailed microstructure in zone 2 along the horizontal direction; (d) the overall microstructure, (e) the detailed microstructure in zone 3, and (f) the detailed microstructure in zone 1 along the building direction.

Furthermore, the microstructures along the horizontal and building directions in the

solutionised alloys without and with subsequent ageing are shown in Fig. 5. The microstructures along the horizontal direction also consisted mostly of equiaxed primary α-Al grains, but the average size increased to 16.25 μm in the as-solutionised sample and 17.26 μm in the as-solutionised and aged sample. Additionally, the melt tracks and Al-cells with eutectic Mg_2Si networks were completely broken up, but still could be traced after solution treatment (Figs. 5b and 5c). The coarsened Mg_2Si particles (~2.5 μm) were dispersed in the Al matrix along both directions. After subsequent ageing at 180 ºC for 2 h, two differences were found in the microstructure: (*i*) the sizes of coarser Mg_2Si particles were similar to that in the as-solutionised sample; (*ii*) the fine *in-situ* Mg_2Si particles were formed in the solutionised and aged sample.

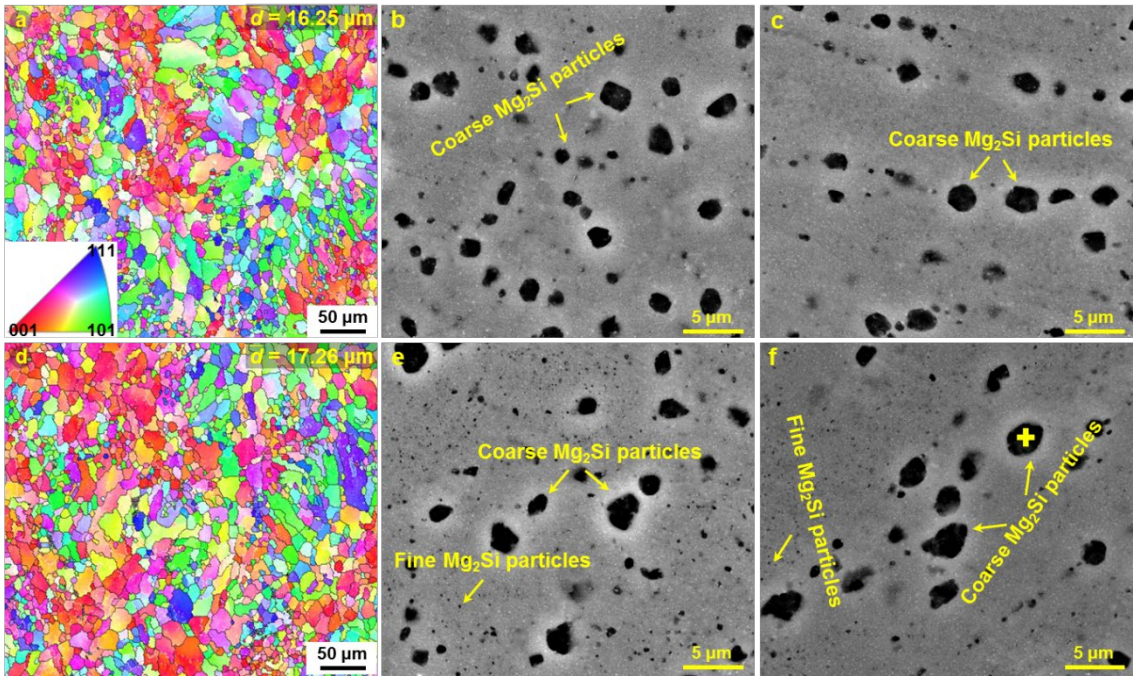

Fig. 5. EBSD images of solutionised Al-5Mg_2Si-2Mg alloy (a) without and (d) with subsequent ageing treatment; SEM images showing (b) the horizontal direction and (c) the building direction of the as-solutionised Al-5Mg_2Si-2Mg alloy, (e) the horizontal direction and (f) the building direction of the solutionised Al-5Mg_2Si-2Mg alloy with subsequent ageing at 180 ºC for 2 h.

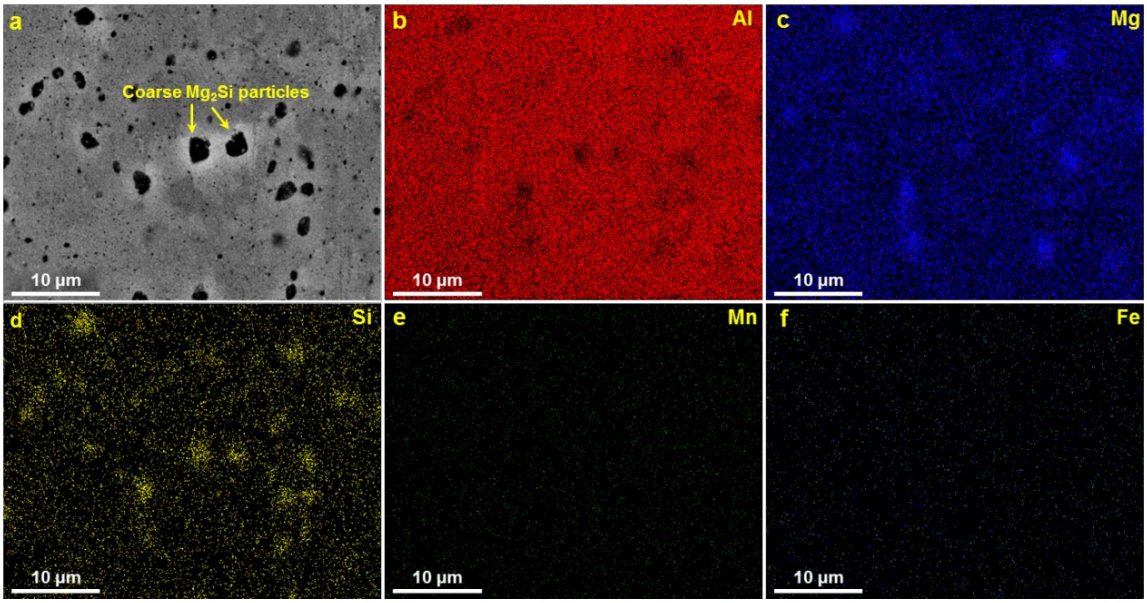

Fig. 6. SEM-EDS mapping images showing the microstructures of as-solutionised and aged Al-5Mg2Si-2Mg alloy for individual element of Al, Mg, Si, Mn and Fe.

Additionally, the chemical composition of coarse particles in the as-solutionised and aged alloy was also evaluated using SEM-EDS. The results of point scan in Fig. 5f and compositional mapping in Fig. 6 showed that these coarsened particles were enriched in Mg and Si, but depleted in Al, confirming the formation of coarse Mg_2Si particles. Therefore, although the coarsened Mg_2Si can weaken the elongation, the reduced residual stress during solution is beneficial for the elongation improvement. On the other hand, the reduced relative density, the broken of Al-Mg_2Si eutectic networks, the coarsened matrix phase, and the worsening of precipitate strengthening resulted from the coarsened Mg_2Si particles would significantly decrease the strength and hardness in the Al-5Mg_2Si-2Mg alloy. Consequently, the solution with and without subsequent ageing is difficult to enhance the strength of L-PBFed Al-5Mg_2Si-2Mg alloy.

Table. 2. EDS results of solutionised and aged alloy corresponding to Fig. 4f and Fig. 5 (in wt.%).

Area	Mg	Si	Mn	Fe	Others	Al
Point in Fig. 5f	60.87	35.81	<0.01	—	—	Bal.
Fig. 6	5.34	2.14	0.33	0.13	<0.08	Bal.

3.2 Effect of direct ageing on the mechanical properties and microstructure

The Vickers hardness of L-PBFed Al-5Mg_2Si-2Mg alloy under as-aged condition is shown in Fig. 7a. The hardness initially increased to peaks, followed by a decrease with prolonged ageing time, showing typical parabolic shape for individual condition. The peaks varied at different ageing temperatures, which were 173.3 Hv at 160 ºC for 6 h , 178.5 Hv at 180 ºC for

3.5 h, and 166.0 Hv at 200 ºC for 3 h. Clearly, the optimal ageing was 180 ºC for 3.5 h. Furthermore, Fig. 7b shows the tensile stress-strain curves of the L-PBFed alloy under different ageing conditions, and the corresponding data is summarized in Table 3. After being aged at optimal condition of 180 ºC for 3.5 h, the UTS, yield strength and elongation were 488 MPa, 377 MPa and 9.6%, respectively. It is clear that the alloy under as-aged condition delivered better comprehensive mechanical properties than that under solutioned and aged condition (Fig. 1b). Thus, direct ageing could be an effective way to enhance the strength of Al-5Mg_2Si-2Mg alloy. Fig. 7c lists the comparison of tensile strength and elongation of the Al-5Mg_2Si-2Mg alloy and other Al-Si-Mg alloys under L-PBFed [22,30–44] and aged/annealed conditions [22,35–44]. Obviously, the aged Al-5Mg_2Si-2Mg alloy in the present work exhibited a giant response for tensile strength. Particularly, the yield strength of the Al-5Mg_2Si-2Mg alloy after ageing at 180 ºC for 3.5 h was higher than those of most hypoeutectic Al-Si-Mg alloys.

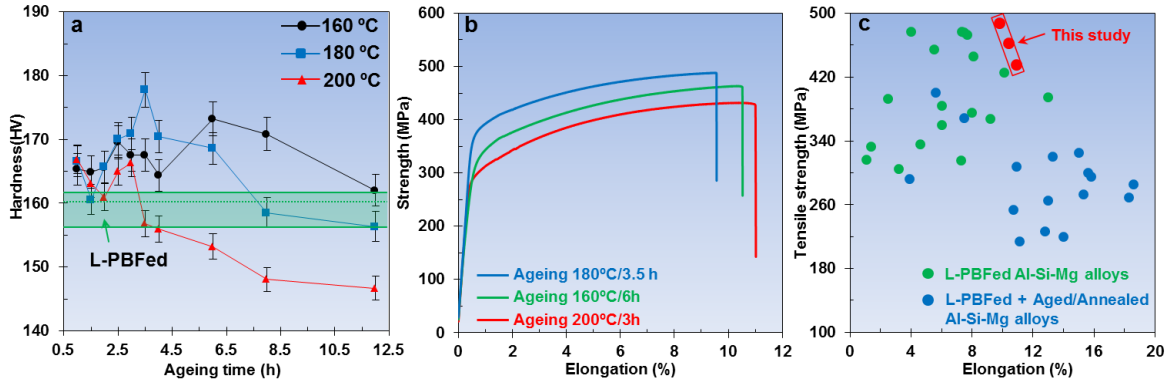

Fig. 7. (a) Ageing time vs. hardness and (b) stress vs. elongation of Al-5Mg_2Si-2Mg alloy under different ageing conditions; (c) Comparison of the tensile properties of the L-PBFed Al-5Mg_2Si-2Mg alloy and other Al-Si-Mg alloys without [22,30–44] and with ageing [22,35–44].

Table 3. The yield strength, UTS, elongation and relative density for the Al-5Mg_2Si-2Mg alloys under different heat treatment conditions.

Condition	Yield strength (MPa)	UTS (MPa)	Elongation (%)	Relative density (%)
As-L-PBFed	295 ± 14	453 ± 11	9.2 ± 2.5	99.25 ± 0.12
Solutionised at 490ºC/1 h	167 ± 10	292 ± 16	17.3 ± 2.6	98.75 ± 0.13
Solutionised + aged at 180 ºC/2 h	191 ± 9	314 ± 13	14.8 ± 2.1	98.48 ± 0.09
Solutionised + aged at 180 ºC/6 h	179 ± 11	295 ± 12	13.2 ± 1.5	98.23 ± 0.11
Aged at 160 ºC/6 h	313 ± 13	464 ± 14	10.5 ± 1.6	99.11 ± 0.14
Aged at 180 ºC/3.5 h	377 ± 16	488 ± 18	9.6 ± 1.8	99.03 ± 0.09
Aged at 200 ºC/3 h	316 ± 11	424 ± 12	11.0 ± 1.9	99.01 ± 0.07

Additionally, the optical micrographs of the L-PBFed Al-5Mg_2Si-2Mg alloy without and with subsequent direct ageing are shown in Fig. 8. The relative density decreased slightly after direct ageing at different temperatures. The relative density decreased from 99.25% under as-LPBFed condition to 99.11% (aged at 160 ºC/6 h), 99.03% (aged at 180 ºC/3.5 h) and 99.01% (aged at 200 ºC/3 h). Furthermore, the fractography of the L-PBFed Al-5Mg_2Si-2Mg alloy under as-aged condition is shown in Fig. 9.The characteristics of fractured surfaces before and after direct ageing were similar. Porosities can be observed in the as-aged samples. As shown in the high-magnification images in Figs. 9e-h, the dimples were relatively shallow and the average dimple size was corresponding to the diameter of eutectic structure of Mg_2Si network. In addition, tearing propagation along grain boundaries was also observed in the as-aged samples, especially in the samples aged at 200 ºC for 3 h, which might be attributed to the effect of over-ageing.

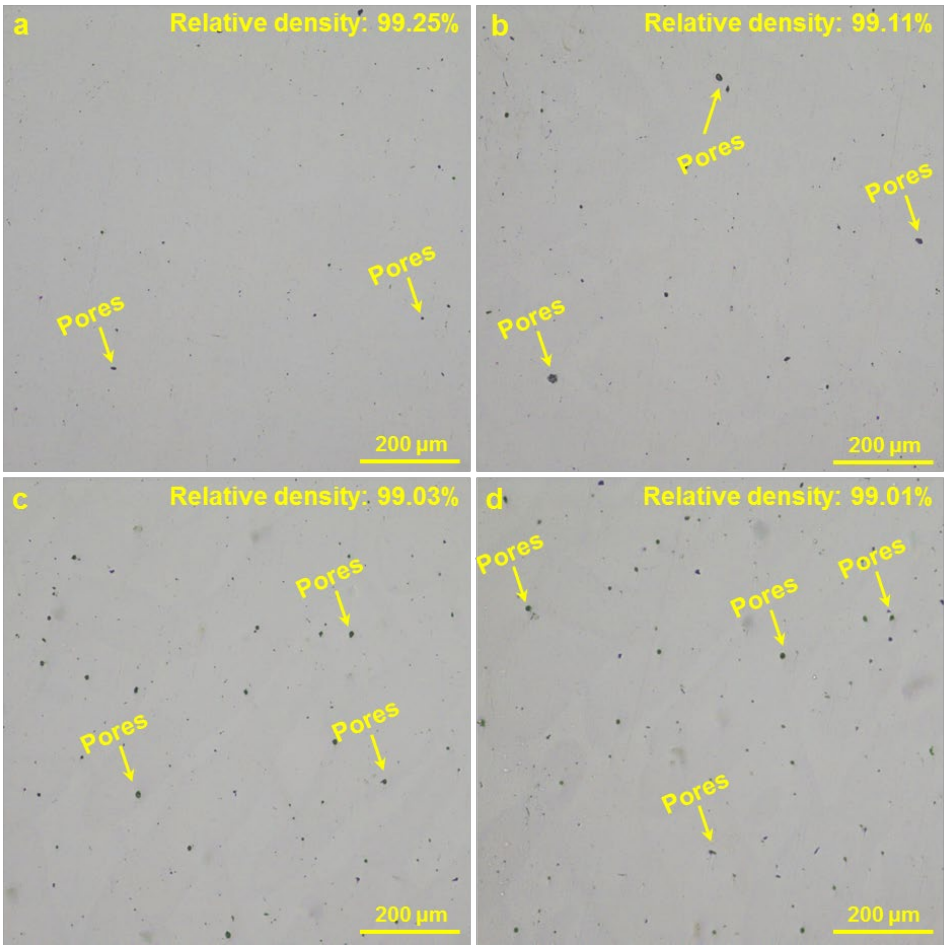

Fig. 8. Optical micrographs of L-PBFed Al-5Mg_2Si-2Mg alloy under different aged conditions, (a) as-LPBFed, (b) aged at 160 ºC/6 h, (c) aged at 180 ºC/3.5 h and (d) aged at 200 ºC/3 h.

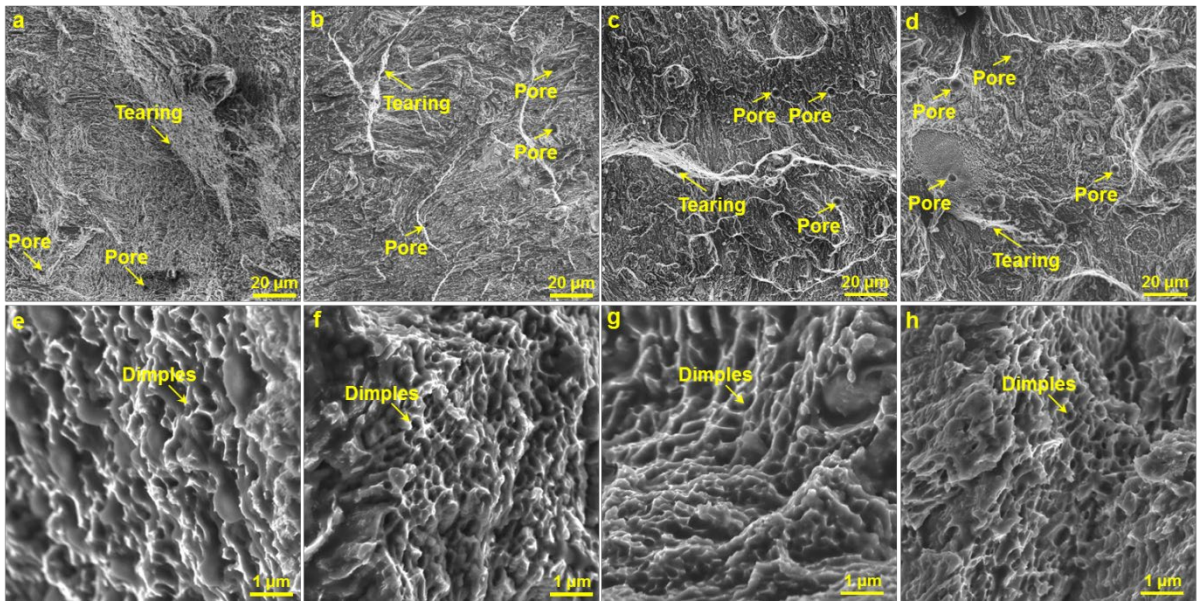

Fig. 9. Tensile fractured morphology of L-BPFed Al-5Mg_2Si-2Mg alloy under different heat treatment conditions, (a,e) as-LPBFed; (b,f) aged at 160 ºC for 6 h; (c,g) aged at 180 ºC for 3.5 h, and (d,h) aged at 200 ºC for 3 h.

The microstructures along the horizontal direction in the directly aged alloys are shown in Fig. 10. Similar to the as-LPBFed alloy, the microstructure under as-aged condition (180 ºC for 3.5 h) consisted mostly of equiaxed primary α-Al grains at a slight coarser size of 15.09 μm, as shown in Fig. 10a. Unlike the as-solutionised alloy, the typical characteristics of Al-Mg_2Si eutectic network with MP zone was not broken under as-aged condition, as shown in Figs. 10b and 10c, respectively. Meanwhile, coarse Al-cells and tiny fine Al-cells could be detected in the centre and edge of MP zone (Figs. 10d and 10e). Most important, the SEM/BSE images in Figs. 10f and 10g confirmed the formation of nano-scale *in-situ* Mg_2Si in the alloy after direct ageing. Additionally, the XRD spectra of the alloys without and with ageing in Fig. 11 also confirmed that the peaks of α-Al and Mg_2Si phases were clearly visible in all samples and no other new phase was observed. Moreover, the peaks of the Mg_2Si phase were weakened in the as-LPBFed samples than that in the as-aged samples, indicating that more Mg_2Si phases were formed after direct ageing, which is also the potential reason that the peak of (111) in the as-LPBF alloy shifts to a higher 2θ angle (Fig. 11b). Thus, the improvement in strength is closely linked with the remained Al-Mg_2Si eutectic network and the formation of *in-situ* Mg_2Si precipitates.

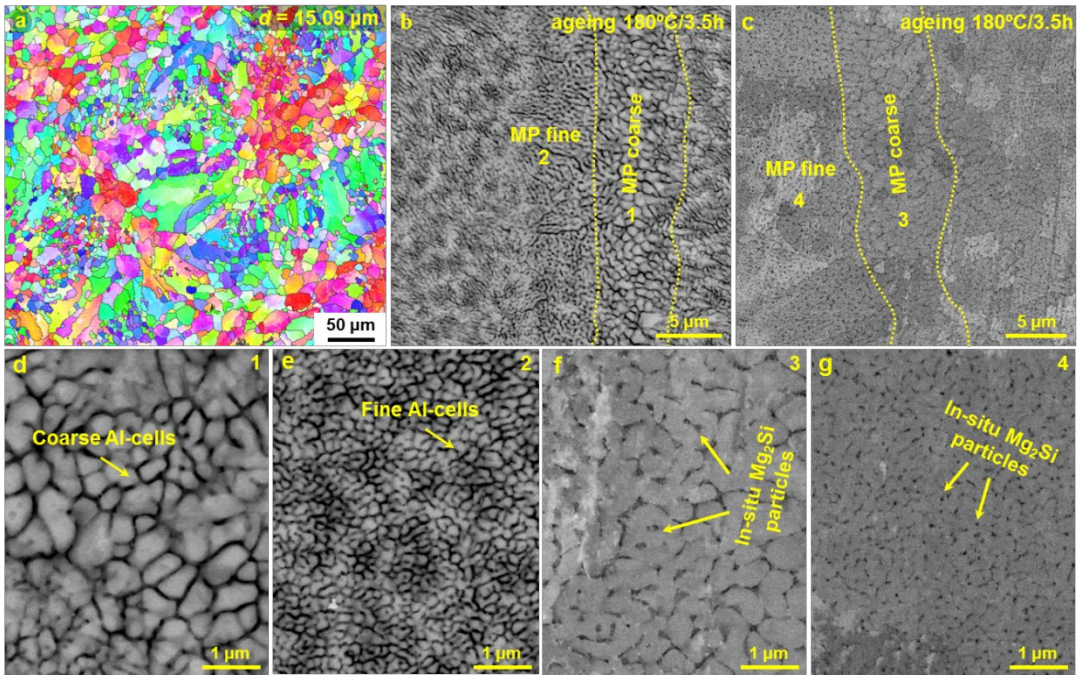

Fig. 10. EBSD images of as-aged Al-5Mg_2Si-2Mg alloy along (a) the horizontal direction (in cross plane parallel to base plate); SEM images showing the overall microstructure (b) with and (c) without etching; (d) the detailed microstructure in the zone 1 of (b); (e) the detailed microstructure in the zone 2 of (b); (f) the detailed microstructure in the zone 3 of (c), and (g) the detailed microstructure in the zone 4 of (c).

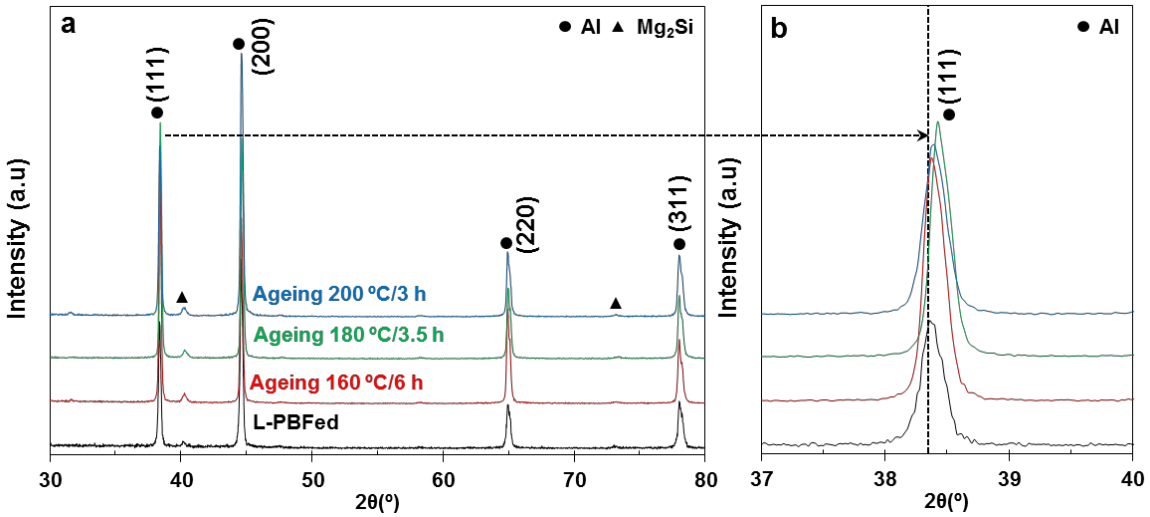

Fig. 11. XRD spectra of L-PBFed Al-5Mg_2Si-2Mg alloy under different ageing conditions of 160 ºC/6 h, 180 ºC/3.5 h and 200 ºC/3 h; (b) details near the (111) peak in (a).

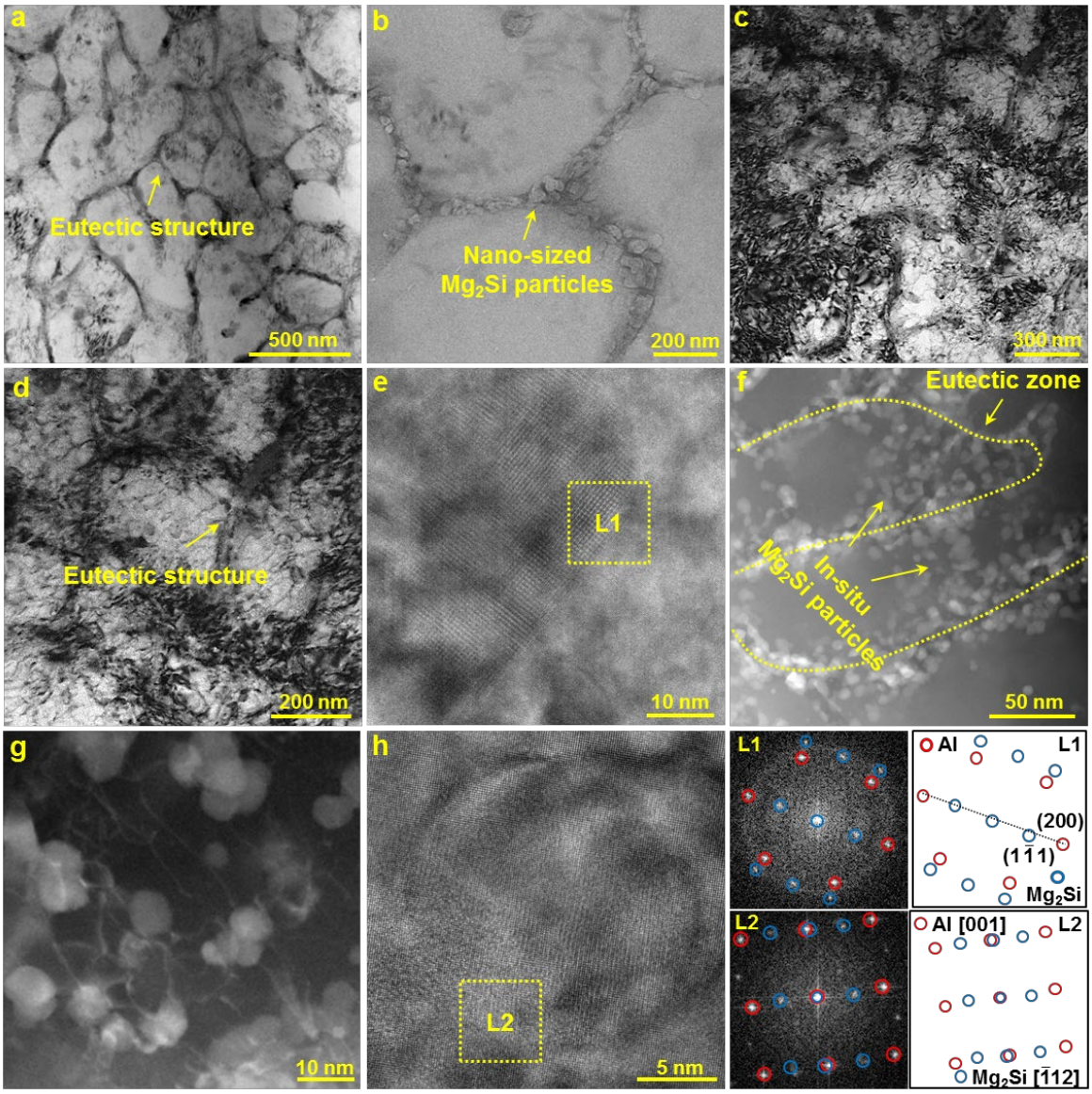

Fig. 12. TEM analysis of L-PBFed Al-5Mg_2Si-2Mg alloy with direct ageing at 180 ºC for 3.5 h; (a,b) BF-TEM images showing the typical Al-Mg_2Si eutectic phase; (c) high density dislocations interacting with the eutectic Mg_2Si phase; (d) the detailed microstructure exhibiting the interaction between dislocations and Mg_2Si particles; (e) HR-TEM image and SAED pattern (L1) showing the interface relationship between α-Al matrix and eutectic Mg_2Si particles. (f) STEM image showing the high density *in-situ* Mg_2Si particles distributed both at boundaries of eutectic phase and within the eutectic phase; (g) the interaction between *in-situ* Mg_2Si particles within eutectic phase and dislocations; (h) HR-TEM image and SAED pattern (L2) showing the interface relationship between α-Al matrix and in-*situ* Mg_2Si particles.

Furthermore, TEM images in Fig. 12 displays the detailed microstructural characteristics along the horizontal direction. The obvious eutectic structure was observed in the bright-field (BF) TEM image in Fig. 12a. Mg_2Si particles formed during L-PBF process with the size of 30 ～ 50 nm was also seen at the boundaries of eutectic structures, as shown in Fig. 12b. Meanwhile, HAADF-STEM images (Fig. 13a, a_1-a_4) demonstrated that Al-cell boundaries

were enriched in Mg and Si elements, further confirming the formation of divorced Al-Mg_2Si eutectics. Moreover, BF-TEM image in Fig. 12c showed that dislocation substructures were well developed in individual Al-cell, and the boundaries of Al-cells comprised a high number density of tangled dislocations, as shown in Fig. 12d, indicating the misorientation of the neighboring Al-cells. Additionally, the high-resolution (HR) TEM in Fig. 12e and fast Fourier transformation (FFT) pattern (L1) indicated that the Al/Mg_2Si interface under the projection direction of $[011]_{Al}//[\bar{1}12]_{Mg2Si}$. The previous study [28] confirmed that the as-LPBFed Al-5Mg_2Si-2Mg alloy was featured by the primary α-Al and the divorced Mg_2Si eutectic networks. After ageing, a large number of nano-sized *in-situ* Mg_2Si particles (about 5～15 nm) were observed both within the Al-cells and at the boundaries of Al-cells (Fig. 12f), which is consistent with the results of XRD in Fig. 11. The subsequent ageing also exhibited strong precipitation strengthening effect induced by the interaction between *in-situ* Mg_2Si nanoparticles with dislocations, as shown in Fig. 12g. Correspondingly, HAADF-STEM images (Fig. 13b, b_1-b_4) demonstrated that the *in-situ* nanoparticles were enriched in Mg and Si elements. The HR-TEM image and FFT pattern of the *in-situ* Mg_2Si particles within Al-cells are shown in Fig. 12h and L2. Obviously, it indicated that the projection direction of $[001]_{Al}//[\bar{1}12]_{Mg2Si}$ between α-Al and *in-situ* Mg_2Si particles.

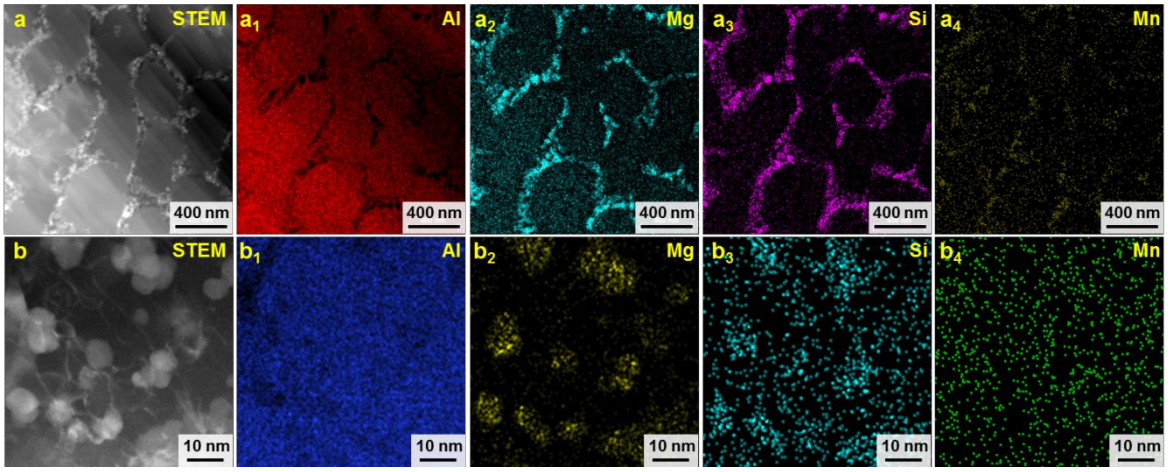

Fig. 13. (a) HAADF-STEM image and (a_1-a_4) the corresponding EDS maps of eutectic microstructure, including the distribution of (a_1) Al; (a_2) Mg; (a_3) Si; and (a_4) Mn; (b) HAADF-STEM image *and* (b_1-b_4) the corresponding EDS maps of the nano-sized Mg_2Si particles precipitated within eutectic, including the distribution of (b_1) Al; (b_2) Mg; (b_3) Si; and (b_4) Mn.

4. Discussion

The results of tensile and hardness results clearly confirmed that the solution treatment of L-PBFed alloy can significantly reduce the strength and increase the elongation. The solution with subsequent ageing is not effective for strength enhancement. The as-LPBFed

Al-5Mg_2Si-2Mg alloy offered the yield strength of 295 MPa, UTS of 453 MPa and elongation of 9.2%. After solution at 490 ºC for 1 h, the alloy exhibits a striking decrease in strength and increase in elongation, at which the yield strength is 167 MPa, the UTS is 292 MPa and the elongation is 17.3%. On the other hand, the direct ageing can significantly improve the strength. Particularly, an optimal combination of mechanical properties (yield strength of 377 MPa, UTS of 488 MPa and elongation of 9.6%) can be achieved in the alloy after ageing at 180 ºC for 3.5 h.

As described in Ref [28] and the results in Figs. 3 and 4, the as-LPBFed Al-5Mg_2Si-2Mg alloys can be strengthened by solid solution hardening, grain refinement and secondary phase strengthening. The high cooling rate in the as-LPBFed alloy can lead to a significant increase in the solid solubility, the supersaturation of Mg_2Si in Al matrix can thus maximize the solid solution strengthening in the Al-5Mg_2Si-2Mg alloy. Also, the strengthening by grain refinement is significant as the results of the combination of heterogeneous nucleation and growth restriction of L-PBF process. This benefits from the formation of fine equiaxed grains, which can be quantitively estimated by Hall-Patch model. The in-situ eutectic Mg_2Si particles are located at the grain boundaries. Large amounts of nanoscale Mg_2Si particles segregated at grain boundaries of Al matrix can impede the boundary sliding under stress. It is also expected that the fine Mg_2Si particles may also promote the dislocation bowing because of the coherency between Mg_2Si and Al matrix, which offer the Orowan strengthening.

The effect of solution on the L-PBFed alloy mainly include the decomposition of the eutectic Mg_2Si phase, which result in the broken of Al-cells and Mg_2Si eutectic phase, blunting and/or sherardizing the sharp Mg_2Si edges and/or tips, dissolving the Mg_2Si phase into Al matrix and the formation of coarse Mg_2Si particles (～2.5 μm), as shown in Figs. 5 and 6. More importantly, nano-sized Mg_2Si particles that were formed during L-PBF processing are disappeared/dissolved into the matrix. Therefore, the strengthening by secondary phases and Orowan is significantly reduced, although the strengthening by solution may be maintained at similar level as that in the as-LPBFed alloy. For the ductility of solutionised alloy, two aspects can be considered. Firstly, the decrease in the number and the increase in size of eutectic Mg_2Si particles are beneficial to the reduction of localized stress or strain. Secondly, solution treatment reduces the residual stresses built up in the as- LPBFed alloy, which has been discussed in with previous studies [20]. As a result, the solutionised samples can provide the significant increase of elongation. Furthermore, the solution heat treatment can significantly increase the porosity level in the sample (Fig. 2), the effect loading area is reduced and the initiation of cracks becomes much easier from the porosity. These are also detrimental factors for the strength. On the other hand, the subsequent ageing of the

solutionised sample cannot form precipitates because of the left shifting of solidus temperature lines and much small concentration variation in the large temperature range in the equilibrium diagram, according to the thermodynamic calculation in ref. [28]. Therefore, the ageing is not able to promote the segregation of solutes atoms to form precipitates. Consequently, the precipitation strengthening is not effective (Fig. 1).

The direct ageing is an effective technique to enhance the mechanical properties, which is also closely linked to the microstructural characteristics. The features of as-aged microstructure include that the refined compact Al-cells and the divorced Mg_2Si eutectic remained the same as that in the as-LPBFed microstructure, but ultrafine in-situ Mg_2Si particles are formed as precipitates (Fig. 10). The results of XRD (Fig. 11) and TEM images (Figs. 12f&g) further confirmed that the precipitation of *in-situ* Mg_2Si after ageing, which can result in the reduction of solid solution strengthening. However, the relatively stronger peak of Mg_2Si under the condition of ageing at 200 ºC for 3 h confirm that the effect of solid solution strengthening is not completely disappeared after ageing at 180 ºC for 3 h; some of the solutes can still offer the solid solution strengthening. Moreover, *in-situ* Mg_2Si nanoparticles are uniform and can offer strengthening through the dislocation by-pass mechanism (Orowan-type) [48] as the dislocations pile up the vicinity of Mg_2Si particles distributed at the boundaries of Al cells. On the other hand, ageing process can reduce the residual stress introduced by the non-uniform temperature distribution and the rapid transition from liquid to solid during L-PBF process [21,36,44,49]. As a result, the strengthening mechanisms that work well for as-LPBFed alloy remained effective in the as-aged alloy. However, more strengthening from precipitates becomes effect as an extra contributor. Consequently, as shown in Fig. 7 and Table 3, the strength in the as-aged alloy is enhanced in comparison that under as-LPBFed, as-solutionised, under solution + aged conditions. In the meantime, the release of residual stress during ageing can lead to an improvement in ductility from 9.2% under as-LPBFed condition to 9.6% under as-LPBFed + aged condition (Fig. 7 and Table 3).

5. Conclusions

a) The as-LPBFed Al-5Mg2Si-2Mg alloy offers the yield strength of 295 MPa, UTS of 453 MPa and elongation of 9.2%. The solution with and without subsequent ageing is not effective for property improvement. After solution at 490 ºC for 1 h, the alloy exhibits a striking decrease in strength and increase in elongation, at which the yield strength is 167 MPa, the UTS is 292 MPa and the elongation is 17.3%. With subsequent ageing at

180 ºC for 6 h, the yield strength is 179 MPa, the UTS is 295 MPa and the elongation is 13.2 %.

b) Direct ageing of as-LPBFed Al-5Mg_2Si-2Mg alloy can significant improve the strength. After ageing at 180 ºC for 3.5 h, the yield strength of 377 MPa, the UTS of 488 MPa and elongation of 9.6% can be achieved in the alloy, showing 28% increase of yield strength in comparison with as-LPBFed alloy, but still with excellent ductility for engineering applications.

c) Solution heat treatment leads to decompose the eutectic Mg_2Si, resulting in the increase of ductility and decrease of yield strength in the as-LPBFed Al-5Mg_2Si-2Mg alloy. More importantly, the solution heat treatment is prone to form porosity, which is detrimental for property enhancement.

d) The characteristics of as-aged microstructure included that the refined compact Al-cells and the divorced Mg_2Si eutectic remained the same as that in the as-LPBFed microstructure, but ultrafine *in-situ* Mg_2Si particles are formed for precipitation strengthening, which is key for the enhancement of yield strength.

CRediT authorship contribution statement

Jianying Wang: Data curation, Writing - original draft, Investigation. **Feipeng Yang:** Investigation, writing - review. **Hailin Yang:** Conceptualization, Funding acquisition, Project administration, Writing - review & editing, Supervision. **Lijun Zhang:** Investigation. **Yingying Zhang:** Investigation. **Zhilin Liu:** Supervision, Writing - review & editing,. **Shouxun Ji:** Conceptualization, Results review, Writing – review & editing.

Declaration of Competing Interest

The authors declare that they have no known competing financial interests or personal relationships that could have appeared to influence the work reported in this paper.

Acknowledgement

Financial support from the National Key Research and Development Program of China (Grant No. 2020YFB0311300ZL), and National Natural Science Foundation of China (Grant No. 52071343) are gratefully acknowledged.

References

[1] R. Prillhofer, G. Rank, J. Berneder, H. Antrekowitsch, P.J. Uggowitzer, S. Pogatscher, Property Criteria for Automotive Al-Mg-Si Sheet Alloys, Materials. 7 (2014) 5047–5068.

[2] T. Hanemann, L.N. Carter, M. Habschied, N.J.E. Adkins, M.M. Attallah, M. Heilmaier, *In-situ* alloying of AlSi10Mg+Si using Selective Laser Melting to control the coefficient of

thermal expansion, J. Alloys. Compd. 795 (2019) 8–18.
[3] O. Engler, J. Hirsch, Texture control by thermomechanical processing of AA6xxx Al-Mg-Si sheet alloys for automotive applications-a review, Mater. Sci. Eng. A 336 (2002) 249–262.
[4] S. Ji, D. Watson, Z. Fan, M. White, Development of a super ductile diecast Al–Mg–Si alloy, Mater. Sci. Eng. A 556 (2012) 824–833.
[5] K. Yamamoto, M. Takahashi, Y. Kamikubo, Y. Sugiura, S. Iwasawa, T. Nakata, S. Kamado, Effect of Mg content on age-hardening response, tensile properties, and microstructures of a T5-treated thixo-cast hypoeutectic Al–Si alloy, Mater. Sci. Eng. A 798 (2020) 140089.
[6] X.L. Izcara, A.G. Blank, F. Pyczak, P. Staron, S. Schumann, N. Huber, Characterization and modelling of the influence of artificial ageing on the microstructural evolution of age-hardenable AlSi10Mg(Cu) aluminium alloys, Mater. Sci. Eng. A 610 (2014) 46–53.
[7] M. Voncina, S. Kores, P. Mrvar, J. Medved, Effect of Ce on solidification and mechanical properties of A360 alloy, J. Alloys Compd. 509 (2011) 7349–7355.
[8] Z.C. Li, Y.L. Deng, M.F. Yuan, J. Zhang, X.B. Guo, Effect of isothermal compression and subsequent heat treatment on grain structures evolution of Al-Mg-Si alloy, J. Cent. South. Univ. 28 (2021) 2670–2686.
[9] X.K. Yang, B.Q. Xiaong, X.W. Li, L.Z. Yan, Z.H. Li, Y.A. Zhang, Y.N. Li, K. Wen, H.W. Liu, Effect of Li addition on mechanical properties and ageing precipitation behavior of extruded Al−3.0Mg−0.5Si alloy, J. Cent. South. Univ. 28 (2021) 2636-2646.
[10] A. Malekan, M. Emamy, J. Rassizadehghani, A.R. Emami, The effect of solution temperature on the microstructure and tensile properties of Al–15%Mg_2Si composite, Mater. Des. 32 (2011) 2701–2709.
[11] J.H. Zhao, L.S. Luo, X. Xue, T. Liu, L. Luo, B.B. Wang, Y.N. Wang, L. Wang, Y.Q. Su, J.J. Guo, H.Z. Fu, The evolution and characterizations of Al3(Sc_xZr_{1-x}) phase in Al–Mg-based alloys proceeded by SLM, Mater. Sci. Eng. A 824 (2021) 141863.
[12] J.L. Zhang, J.B. Gao, B. Song, L.J. Zhang, C.J. Han, C. Cai, K. Zhou, Y.S. Shi, A novel crack-free Ti-modified Al-Cu-Mg alloy designed for selective laser melting, Addit. Manuf. 38 (2021) 101829.
[13] Q.B. Jia, F. Zhang, P. Rometsch, J.W. Li, J. Mata, M. Weyland, L. Bourgeois, M. Sui, X.H. Wu, Precipitation kinetics, microstructure evolution and mechanical behavior of a developed Al–Mn–Sc alloy fabricated by selective laser melting, Acta Mater. 193 (2020) 239–251.
[14] B. Jiang, Y.B. Chen, X. Chen, M.D. Starostenkov, G.J. Dong, Densification, microstructural features and tensile properties of selective laser melted AlMgSiScZr alloy from single track to block specimen, J. Cent. South. Univ. 28 (2021) 1129–1143.
[15] E.O. Olakanmi, R.F. Cochrane, K.W. Dalgarno, A review on selective laser sintering/melting (SLS/SLM) of aluminium alloy powders: processing, microstructure, and properties, Prog. Mater. Sci. 74 (2015) 401–477.

[16] U. Patakham, A. Palasay, P. Wila, R. Tongsri, MPB characteristics and Si morphologies on mechanical properties and fracture behavior of SLM AlSi10Mg, Mater. Sci. Eng. A 21 (821) 141602.
[17] J. Suryawanshi, K.G. Prashanth, S. Scudino, J. Eckert, O. Prakash, U. Ramamurty, Simultaneous enhancements of strength and toughness in an Al-12Si alloy synthesized using selective laser melting, Acta Mater. 115 (2016) 285–294.
[18] C. Gao, W. Wu, J. Shi, Z. Xiao, A.H. Akbarzadeh, Simultaneous enhancement of strength, ductility, and hardness of TiN/AlSi10Mg nanocomposites via selective laser melting, Addit. Manuf. 34 (2020) 101378.
[19] H. Rao, S. Giet, K. Yang, X. Wu, C. Davies, The influence of processing parameters on aluminium alloy A357 manufactured by selective laser melting, Mater. Des. 109 (2016) 334–346.
[20] X.P. Li, X.J. Wang, M. Saunders, A. Suvorova, L.C. Zhang, Y.J. Liu, M.H. Fang, Z.H. Huang, T.B. Sercombe, A selective laser melting and solution heat treatment refined Al-12Si alloy with a controllable ultrafine eutectic microstructure and 25% tensile ductility, Acta Mater. 95 (2015) 74–82.
[21] K.G. Prashanth, S. Scudino, J. Eckert, Defining the tensile properties of Al-12Si parts produced by selective laser melting, Acta Mater. 126 (2017) 25–35.
[22] I. Rosenthal, R. Shneck, A. Stern, Heat treatment effect on the mechanical properties and fracture mechanism in AlSi10Mg fabricated by additive manufacturing selective laser melting process, Mater. Sci. Eng. A 729 (2018) 310–322.
[23] W.H. Kan, Y. Nadot, M. Foley, L. Ridosz, G. Proust, J.M. Cairney, Factors that affect the properties of additively-manufactured AlSi10Mg: porosity versus microstructure, Addit. Manuf. 29 (2019) 100805.
[24] P. Wang, C. Gammer, F. Brenne, K. G. Prashanth, R.G. Mendes, M.H. Rümmeli, T. Gemming, J. Eckert, S. Scudino, Microstructure and mechanical properties of a heat-treatable Al-3.5Cu-1.5Mg-1Si alloy produced by selective laser melting, Mater. Sci. Eng. A 711 (2018) 562–570.
[25] Q.Y. Tan, J.Q. Zhang, Q. Sun, Z.Q. Fan, G. Li, Y. Yin, Y.G. Liu, M.X. Zhang, Inoculation treatment of an additively manufactured 2024 aluminium alloy with titanium nanoparticles, Acta Mater. 196 (2020) 1–16.
[26] Y. Shi, K. Yang, S.K. Kairy, F. Palm, X. Wu, P.A. Rometsch, Effect of platform temperature on the porosity, microstructure and mechanical properties of an Al–Mg–Sc–Zr alloy fabricated by selective laser melting, Mater. Sci. Eng. A 732 (2018) 41–52.
[27] R.D. Li, M.B. Wang, Z.M. Li, P. Cao, T.C. Yuan, H.B. Zhu, Developing a high-strength Al-Mg-Si-Sc-Zr alloy for selective laser melting: Crack-inhibiting and multiple strengthening mechanisms, Acta Mater. 193 (2020) 83–98.
[28] H.L. Yang, Y.Y. Zhang, J.Y. Wang, Z.L. Liu, C.H. Liu, S.X. Ji, Additive manufacturing of a high strength Al-5Mg_2Si-2Mg alloy: Microstructure and mechanical properties, J. Mater. Sci. Tech. 91 (2021) 215–223.

[29] F. Yan, W.C. Yang, S.X. Ji, Z.Y. Fan, Effect of solutionising and ageing on the microstructure and mechanical properties of a high strength die-cast Al-Mg-Zn-Si alloy, Mater. Chem. Phys. 167 (2015) 88–96.
[30] J.H. Martin, B.D. Yahata, J.M. Hundley, J.A. Mayer, T.A. Schaedler, T.M. Pollock, 3D printing of high-strength aluminium alloys, Nature. 549 (2017) 365.
[31] N. Read, W. Wang, K. Essa, M.M. Attallah, Selective laser melting of AlSi10Mg alloy: process optimisation and mechanical properties development, Mater. Des. 65 (2015) 417–424.
[32] P. Wei, Z.Y. Wei, Z. Chen, J. Du, Y.Y. He, J.F. Li, Y.T. Zhou, The AlSi10Mg samples produced by selective laser melting: Single track, densification, microstructure and mechanical behaviour, Appl. Surf. Sci. 408 (2017) 38–50.
[33] B. Chen, S.K. Moon, X. Yao, K. Kondoh, Strength and strain hardening of a selective laser melted AlSi10Mg alloy, Scr. Mater. 141 (2017) 45–49.
[34] N.E. Uzan, R. Shneck, O. Yeheskel, N. Frage, Fatigue of AlSi10Mg specimens fabricated by additive manufacturing selective laser melting (AM-SLM), Mater. Sci. Eng. A 704 (2017) 229–237.
[35] T. Kimura, T. Nakamoto, Microstructures and mechanical properties of A356 (AlSi7Mg0.3) aluminium alloy fabricated by selective laser melting, Mater. Des. 89 (2016) 1294–1301.
[36] M. Wang, B. Song, Q.S. Wei, Y.J. Zhang, Y.S. Shi, Effects of annealing on the microstructure and mechanical properties of selective laser melted AlSi7Mg alloy, Mater. Sci. Eng. A 739 (2019) 463–472.
[37] N.T. Aboulkhair, I. Maskery, C. Tuck, I. Ashcroft, N.M. Everitt, The microstructure and mechanical properties of selectively laser melted AlSi10Mg: The effect of a conventional T6-like heat treatment, Mater. Sci. Eng. A 667 (2016) 139–146.
[38] N. Takata, H. Kodaira, K. Sekizawa, A. Suzuki, M. Kobash, Change in microstructure of selectively laser melted AlSi10Mg alloy with heat treatments, Mater. Sci. Eng. A 704 (2017) 218–228.
[39] K.V. Yang, P. Rometsch, C.H.J. Davies, A.J. Huang, X.H. Wu, Effect of heat treatment on the microstructure and anisotropy in mechanical properties of A357 alloy produced by selective laser melting, Mater. Des. 154 (2018) 275–290.
[40] S. Bagherifard, N. Beretta, S. Monti, M. Riccio, M. Bandini, M. Guagliano, On the fatigue strength enhancement of additive manufactured AlSi10Mg parts by mechanical and thermal post-processing, Mater. Des. 145 (2018) 28–41.
[41] L.C. Zhuo, Z.Y. Wang, H.J. Zhang, E.H. Yin, Effect of post-process heat treatment on microstructure and properties of selective laser melted AlSi10Mg alloy, Mater. Lett. 234 (2019) 196–200.
[42] D.H. Dai, D.D. Gu, H. Zhang, J.Y. Zhang, Y.X. Du, T. Zhao, C. Hong, A. Gasser, R. Poprawe, Heat-induced molten pool boundary softening behaviour and its effect on tensile properties of laser additive manufactured aluminium alloy, Vacuum 154 (2018) 341–350.

[43] C.C. Zhang, H.H. Zhu, H.L. Liao, X.Y. Zeng, Effect of heat treatments on fatigue property of selective laser melting AlSi10Mg, Int. J. Fatigue 116 (2018) 513–522.
[44] N. Takata, M.L. Liu, H. Kodaira, A. Suzuki, M. Kobashi, Anomalous strengthening by supersaturated solid solutions of selectively laser melted Al-Si-based alloys, Addit. Manuf. 33 (2020) 101152.
[45] H. Zhang, Y. Wang, J.J. Wang, D.R. Ni, D. Wang, B.L. Xiao, Z.Y. Ma, Achieving superior mechanical properties of selective laser melted AlSi10Mg via direct aging treatment, J. Mater. Sci. Tech. 108 (2022) 226–235.
[46] H. Wu, Y.J. Ren, J.Y. Ren, L.X. Liang, R.D. Li, Q.H. Fang, A.H. Cai, Q. Shan, Y.T. Tian, I. Baker, Selective laser melted AlSi10Mg alloy under melting mode transition: Microstructure evolution, nanomechanical behaviors and tensile properties, J. Alloys. Compds. 873 (2021) 159823.
[47] R. Geng, F. Qiu, Q.L. Zhao, Y.Y. Gao, Q.C. Jiang, Effects of nanosized TiCp on the microstructure evolution and tensile properties of an Al-Mg-Si alloy during cold rolling, Mater. Sci. Eng. A 743 (2019) 98–105.
[48] P.M. Hazzledine, Direct versus indirect dispersion hardening, Scripta. Metall. Mater. 26 (1992) 57–58.
[49] Y. Bai, Y. Yang, Z. Xiao, M. Zhang, D. Wang, Process optimization and mechanical property evolution of AlSiMg0.75 by selective laser melting, Mater. Des. 140 (2018) 257–266.